Unlocking time-dependent CP violation without signal vertexing at B factories

M. Dorigo , ¹ S. Raiz , ² D. Tonelli , ¹ and R. Žlebčík ¹ INFN Sezione di Trieste, Trieste, Italy ² Deutsches Elektronen-Synchrotron (DESY), Hamburg, Germany

We present a method to measure time-dependent CP violation in B^0 decays produced in $\Upsilon(4S) \to B^0 \overline{B}^0$ events at B factories without reconstructing the signal decay vertex. The method exploits the sensitivity of the tag \overline{B}^0 decay time to CP violation in the B^0 signal. It relies on a compact e^+e^- interaction region and excellent vertex resolution, which enable precise measurement of the displacement between production and decay vertices of the tag meson. We study an application to $B^0 \to \pi^0\pi^0$ decays using a simplified simulation that approximates the conditions of the Belle II experiment at the SuperKEKB collider. Our approach achieves a sensitivity on mixing-induced CP violation that would require 20 times larger samples with standard approaches. When incorporated into the $B \to \pi\pi$ isospin analysis, the expected results would reduce the degeneracy of ϕ_2 solutions and significantly increase precision. This work opens a path to previously inaccessible CP-violation studies enhancing and accelerating the reach of Belle II and future flavor physics programs.

I. INTRODUCTION

Measurements of decay-rate asymmetries that violate the combined transformation of charge conjugation and parity (CP symmetry) are central to the study of the weak interactions of quarks. These measurements provide stringent tests of the Cabibbo-Kobayashi-Maskawa (CKM) mechanism, which prescribes that all CP-violating phenomena in the standard model of particle physics are accommodated by a single complex phase in the quark couplings with W^{\pm} bosons [1]. For neutral strange, charm, and bottom mesons, CP violation phenomenology is further enriched by particle-antiparticle oscillations, vielding CP-violating decay-rate asymmetries that depend on meson decay time. The observation of these asymmetries in the $B^0 \to J/\psi K^0$ decays provided the conclusive experimental confirmation of the CKM paradigm in the early 2000s [2, 3]. The focus then shifted toward using time-dependent CP violation as a sensitive probe for physics beyond the standard model (see, e.g., Ref. [4] and references therein).

Bottom mesons have been extensively studied at experiments in energy-asymmetric electron-positron collisions near the $\Upsilon(4S)$ resonance (so-called B factories), such as BaBar, Belle, and Belle II, as well as hadron-collider experiments, such as CDF, D0, LHCb, CMS, and AT-LAS [5]. Two ingredients are essential for measuring time-dependent CP asymmetries: determining whether the oscillating meson is a B^0 or a \overline{B}^0 (i.e., flavor) at a known time before decay, and measuring the proper-time interval between that instant and the decay. The experimental approaches to flavor determination—and thus to establishing the relevant time—differ significantly between B factories and hadron colliders.

At hadron-collider experiments, B^0 and \overline{B}^0 mesons originate from the hadronization of incoherently produced $b\overline{b}$ quark pairs. Flavor tagging is performed at production (see, e.g., Refs [6–8]) and the *CP*-violating decay-rate asymmetry depends only on the signal decay time, which is measured from the observed distance be-

tween its production and decay positions and its momentum.

At B factories, neutral bottom mesons are produced in quantum-entangled $B^0\overline{B}^0$ pairs through the process $e^+e^- \to \Upsilon(4S) \to B^0\overline{B}^0$, where the e^+ and e^- beams have different energies, boosting the $\Upsilon(4S)$ in the laboratory frame. The entangled pair evolves coherently until one meson decays, at which time the two flavors are opposite. Then, the remaining meson evolves until it decays. If one meson, identified as $B_{\rm tag}$, decays into a final state that unambiguously defines its flavor and the other, B_{CP} , decays into a final state accessible to both flavors, a measurement of time-dependent CP violation for B_{CP} is possible (see, e.g., Ref. [9]). The corresponding time-evolution and CP-violating decay-rate asymmetry are described in terms of the flavor correlations between the two mesons and

$$\Delta t = t_{CP} - t_{\text{tag}},\tag{1}$$

the difference between the two decay times, which can be either positive or negative. This difference is measured from the spatial separation of the two decay positions using the known boost.

In this paper, we present a method to measure time-dependent CP-violating asymmetries at B factories for decays in which Δt is not available because the B_{CP} decay position is not reconstructed. This limitation arises when the final state includes only neutral particles such as photons or K^0 mesons as in $B^0 \to \pi^0 \pi^0$, $B^0 \to K^0 \pi^0 (\pi^0)$, $B^0 \to K^0 \overline{K}^0 (K^0)$, or the yet-unobserved $B^0 \to \gamma \gamma$ decays. Similar ideas have been explored in the past [10].

In B^0 decays involving neutral pions, the π^0 is typically reconstructed via $\pi^0 \to \gamma\gamma$, which provides no vertex information. Processes like $\pi^0 \to e^+e^-\gamma$, whether from Dalitz decays or photon conversions, enable signal-vertex reconstruction, but their low branching fractions, $\mathcal{O}(10^{-2})$, make measurements of time-dependent CP violation feasible only with extremely large data samples. In B^0 decays involving neutral kaons, no K_L^0 decays and only the fraction of $K_S^0 \to \pi^+\pi^-$ decays that occur in the

inner volume of silicon-vertex detectors provides precise signal-vertex information. In B^0 decays into photons, only conversions can be used, resulting in severe sample-size limitations.

Our approach overcomes these limitations, enabling sensitive measurement of time-dependent CP violation in samples that are already available. The approach relies solely on determining $t_{\rm tag}$, from the displacement between the $B_{\rm tag}$ production and decay points, in analogy with decay-time reconstruction in hadron collisions. However, it exploits the intrinsic connection of $t_{\rm tag}$ to the B_{CP} asymmetry due to the quantum-entangled nature of the $B^0\overline{B}^0$ pair characteristic of B factories.

Key to our method is the resolution of the measurement of the $B_{\rm tag}$ production and decay positions. The latter depends on detector design and performance and it is important because it contributes to the precision on the measurement. However, the former, which depends on the features of the e^+e^- interaction region (IR), is a dominant limiting factor. The entire feasibility of the method is driven by the following collider-specific enablers: a small IR transverse size, a nonzero crossing angle for the beams, and a sufficient $\Upsilon(4S)$ boost.

We first describe the approach with an analytical derivation based on the standard formalism of time-evolution of quantum-entangled $B^0\overline{B}^0$ pairs. We then use simplified simulated experiments that approximate the experimental conditions of the Belle II experiment at the SuperKEKB collider to demonstrate quantitatively the performance with a specific case of interest: the measurement of the time-dependent CP asymmetry in $B^0 \to \pi^0\pi^0$ decays. Natural units are used, with $\hbar = c = 1$, throughout the paper.

II. TIME-DEPENDENT ASYMMETRY FROM THE TAG DECAY TIME

In a B factory experiment, the time-dependent decay rate into a CP eigenstate of a neutral B meson is [9]

$$\mathcal{P}(\Delta t, q) = \frac{e^{-|\Delta t|/\tau}}{4\tau} \left(1 + q \left[S \sin \Delta m \Delta t - C \cos \Delta m \Delta t \right] \right), \tag{2}$$

where we assume CPT invariance (T being the time-reversal transformation) and neglect a small lifetime difference between the two B physical states, which have a mass difference Δm and lifetime τ . The signal decay rate differs for B^0 and \overline{B}^0 according to the $B_{\rm tag}$ flavor q at $\Delta t = 0$ ps. The flavor q equals either +1 for $B_{\rm tag} = B^0$ or -1 for $B_{\rm tag} = \overline{B}^0$. Such a difference generates a nonzero time-dependent CP-violating asymmetry,

$$\mathcal{A}_{CP}(\Delta t) = \frac{\mathcal{P}(\Delta t, +1) - \mathcal{P}(\Delta t, -1)}{\mathcal{P}(\Delta t, +1) + \mathcal{P}(\Delta t, -1)}$$

$$= S \sin \Delta m \Delta t - C \cos \Delta m \Delta t.$$
(3)

when either of the CP-violating coefficients S or C, which are functions of the relevant combinations of quark couplings involved in the transition, differ from zero.

Our method relies solely on the measurement of t_{tag} . We write the probability of observing a signal meson decaying at time t_{CP} accompanied by a partner B_{tag} with flavor q decaying at time t_{tag} , with both times measured relative to the instant of the $\Upsilon(4S)$ decay [10, 11],

$$\mathcal{P}(t_{\text{tag}}, t_{CP}, q) = \frac{e^{-\frac{t_{CP} + t_{\text{tag}}}{\tau}}}{2\tau^2} \left(1 + q \left[S \sin \Delta m (t_{CP} - t_{\text{tag}}) - C \cos \Delta m (t_{CP} - t_{\text{tag}}) \right] \right),$$

$$(4)$$

and then integrate it over the unobserved signal decaytime t_{CP} to obtain the dependence on t_{tag} only and express it in a form that resembles Eq. (2),

$$\mathcal{P}(t_{\text{tag}}, q) = \frac{e^{-t_{\text{tag}}/\tau}}{2\tau} \left(1 + q \left[S' \sin \Delta m (t_{\text{tag}} - \hat{t}) \right] - C' \cos \Delta m (t_{\text{tag}} - \hat{t}) \right] \right), \tag{5}$$

in which

$$\hat{t} = \frac{1}{\Delta m} \arctan(\Delta m \tau) \approx 1.294 \,\mathrm{ps}.$$
 (6)

The corresponding time-dependent CP asymmetry is

$$\mathcal{A}'_{CP}(t_{\text{tag}}) = S' \sin \Delta m(t_{\text{tag}} - \hat{t}) - C' \cos \Delta m(t_{\text{tag}} - \hat{t}),$$
(7)

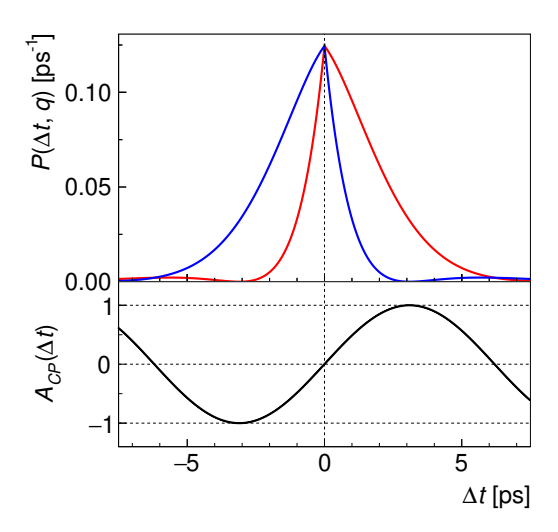
in which

$$S' = -\frac{S}{\sqrt{1 + (\tau \Delta m)^2}}, \quad C' = \frac{C}{\sqrt{1 + (\tau \Delta m)^2}}.$$
 (8)

Figure 1 compares the standard decay rate $\mathcal{P}(\Delta t, q)$ and the rate $\mathcal{P}(t_{\rm tag}, q)$ obtained by only observing $t_{\rm tag}$, along with the corresponding asymmetries $\mathcal{A}_{CP}(\Delta t)$ and $\mathcal{A}'_{CP}(t_{\rm tag})$, for S=1.0 and C=0.0. The mass difference and the lifetime are set to the values known for the B^0 meson [12]. The standard CP asymmetry $\mathcal{A}_{CP}(\Delta t)$ is reduced to an asymmetry $\mathcal{A}'_{CP}(t_{\rm tag})$, whose maximum amplitude is smaller by a factor

$$\frac{1}{\sqrt{1 + (\tau \Delta m)^2}} \approx 0.792. \tag{9}$$

The advantage of using Δt , when both t_{CP} and $t_{\rm tag}$ are available, is that the amplitude of the time-dependent oscillation is not damped and reaches a maximum earlier in time. However, time-dependent CP violation remains accessible, though reduced, if the decay vertex of B_{CP} is not reconstructed. The reduction is the combined effect of the dampening of the asymmetry and the shift of its maximum value to higher decay times by \hat{t} , which result



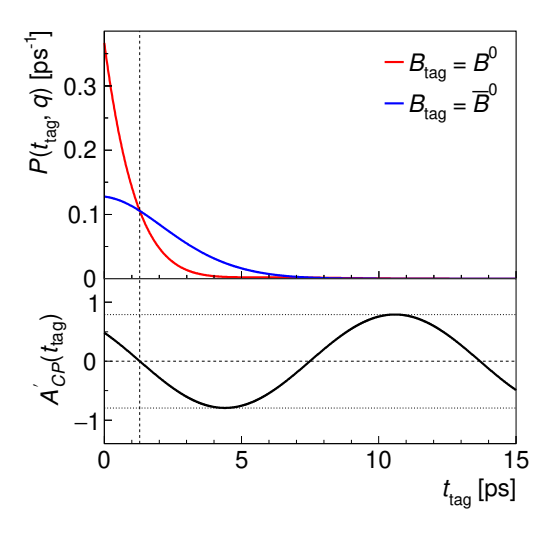


Figure 1. (Top panels) Theoretical decay rates as a function of (left) Δt and (right) $t_{\rm tag}$, for tagged (blue) B^0 and (red) \overline{B}^0 mesons assuming S=1.0 and C=0.0. (Bottom panels) corresponding CP-violating decay-rate asymmetries (left) $\mathcal{A}_{CP}(\Delta t)$ and (right) $\mathcal{A}'_{CP}(t_{\rm tag})$. The horizontal dashed lines show the maximum oscillation amplitudes. The vertical dashed line shows (left) the Δt origin and (right) the \hat{t} value in Eq. (6). The decay time $t_{\rm tag}$ is non-negative by definition.

in a smaller yield. Note that Eqs. (5) and (7) also apply to B_{CP} , when replacing t_{tag} with t_{CP} and inverting the sign of S'.

When measuring time-dependent CP violation, three experimental effects influence the standard asymmetry $\mathcal{A}_{CP}(\Delta t)$ and must also be considered for $\mathcal{A}'_{CP}(t_{\text{tag}})$. Tag-side interference [13] is expected to induce a small bias and is therefore neglected in the following. The other two effects reduce the observable asymmetry and are more relevant: the efficiency for assigning the correct flavor and the resolution on the time measurement.

Considering a fraction w of events with wrong flavor assignment, the amplitude of the time-dependent CP asymmetry is reduced by a factor 1-2w. The corresponding dilution of the sensitivity to the asymmetry is expressed by the effective flavor-tagging efficiency, a factor that scales the actual signal-sample size down to the fraction that is effectively sensitive to the decay-rate asymmetry. The effective flavor-tagging efficiency is typically 35% at B factories [9, 14].

Dilution due to time resolution is the dominant limitation to the sensitivity to $\mathcal{A}'_{CP}(t_{\mathrm{tag}})$ as misreconstructing the time clearly degrades the observed time modulation. Figure 2 shows uncertainties on the CP-violating coefficients S and C as functions of the resolution on either t_{tag} , in the case of the asymmetry $\mathcal{A}'_{CP}(t_{\mathrm{tag}})$, or Δt , in the case of a standard asymmetry $\mathcal{A}_{CP}(\Delta t)$. To single out the relevant dependence, here we are assuming a signal-only sample of 10^3 perfectly flavor-tagged decays. Resolutions are intended as the widths of the relevant Gaussian functions. All uncertainties increase as the resolution on the relevant time measurement worsens. When both the tag and signal vertices are available, the uncertainties with the t_{tag} -based approach are worse than those with the standard Δt -based method, because

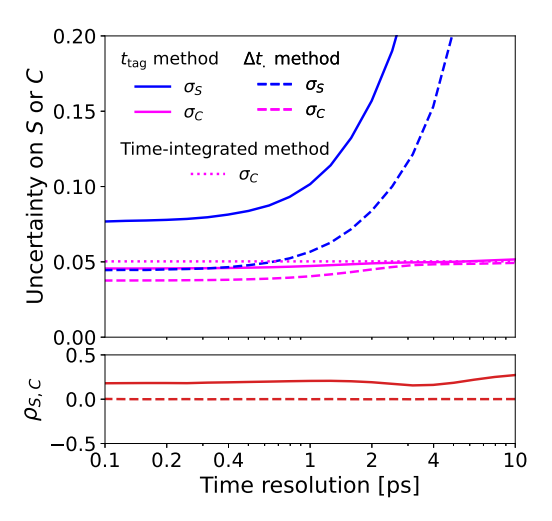


Figure 2. (Top panel) uncertainties on the CP-violating coefficients (blue) S and (magenta) C as functions of the resolution on (solid line) $t_{\rm tag}$ or (dashed line) Δt , for 10^3 perfectly-tagged signal-only decays. (Bottom panel) Linear correlation between the coefficients.

of the dampening effects from Eq. 9 and the time shift \hat{t} of $\mathcal{A}'_{CP}(t_{\rm tag})$. The C uncertainties depend weakly on the time resolution and saturate at the level expected in a time-integrated measurement, which is feasible because, for B^0 mesons, the oscillation period is comparable to their lifetime. As a result, the cosine term in the asymmetry of Eq. (3) does not average out. The time-integrated asymmetry is, however, reduced by a factor $1-2\chi$, where $\chi=(\Delta m\,\tau)^2/[2(1+(\Delta m\,\tau)^2)]\approx 0.18$. The S uncertainties are nearly constant up to a resolution of about 0.5 ps. At poorer time resolutions, they deteriorate

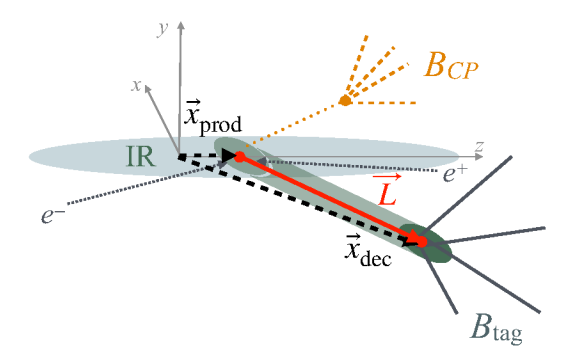


Figure 3. Sketch of a $B^0\overline{B}^0$ event topology in the vicinity of the interaction region. Nothing is to scale.

as expected from the damping of the oscillation amplitude, which is approximately $\exp[-(\Delta m \sigma)^2/2]$, where σ is the time resolution [15]. Figure 2 shows also the linear correlation between S and C as a function of the time resolution. In measurements based on $t_{\rm tag}$, the correlation is nonzero (approximately 20%) because the restriction $0 < t_{\rm tag} < +\infty$ does not allow the cancellation of correlations between negative and positive Δt that occurs in the standard method.

The resolution on Δt is about 0.5 ps at Belle II and around 1.0 ps in Belle and Babar [14, 16, 17]. The resolutions on $t_{\rm tag}$ are generally expected to be worse, as they critically depend not only on accurately determining the $B_{\rm tag}$ decay point, but also its production point, unlike in the standard method.

III. MEASUREMENT OF THE TAG DECAY TIME

The production and decay space-points of the B_{tag} meson identify a flight-distance vector, \vec{L} . The B_{tag} decay time

$$t_{\text{tag}} = m_B \frac{\vec{L} \cdot \vec{p}_{\text{tag}}}{|p_{\text{tag}}|^2}, \tag{10}$$

in which m_B is the known B^0 mass, is reconstructed by projecting the flight distance onto the $\vec{p}_{\rm tag}$ momentum direction, to average out minor direction biases due to experimental inaccuracies. In typical measurements of time-dependent CP violation, the decay of the signal B_{CP} meson is fully reconstructed, and therefore the momentum \vec{p}_{CP} is known. This holds independently of the availability of signal vertex information. The momentum of the partner $B_{\rm tag}$ meson is therefore inferred as $\vec{p}_{\rm tag} = \vec{p}_{\Upsilon(4S)} - \vec{p}_{CP}$, where $\vec{p}_{\Upsilon(4S)}$ is the momentum of the $\Upsilon(4S)$ meson in the $e^+e^- \to \Upsilon(4S) \to B^0\bar{B}^0$ process, which is known precisely from the accelerator pa-

	Belle II	Belle	BaBar
e^- (e^+) beam energy [GeV]	7.0 (4.0)	8.0 (3.5)	9.0(3.0)
Beam energy spread [MeV]	5.45	5.36	4.63
Crossing angle [mrad]	83	22	0
Interaction region x width $[\mu m]$	13	70	148
Interaction region y width $[\mu m]$	0.2	1.0	6.9
Interaction region z width [μ m]	350	6000	15150
B_{tag} vertex x-y resolution [μ m]	30	80	80
$B_{\rm tag}$ vertex z resolution [μ m]	30	100	125

Table I. Summary of B factory parameters relevant for the measurement of $t_{\rm tag}$ [17–23].

rameters. All momenta are measured in the laboratory reference frame.

The precision on \vec{L} depends on the precision on the B_{tag} production and decay space-points, and usually drives the precision on the time measurement, as the fractional uncertainty on the momentum is typically much smaller.

The precision on the B_{tag} production and decay spacepoints depends on the details of the interaction region. At B factories, the IRs are typically ellipsoidal, with major axes approximately aligned with the beam directions, which define the z axes of the coordinate systems (see Fig. 3). The IR spatial dimensions are specific to each collider and are typically determined using processes such as $e^+e^- \to \mu^+\mu^-$ [18]. They can generally be modeled in each spatial direction by a Gaussian distribution, whose width represents the spatial extent of the IR core along that direction. Typical IR widths for the SuperKEKB (Belle II), KEKB (Belle), and PEP-II (BaBar) colliders are listed in Table I. The IR dispersions along the x and y directions are particularly relevant to the precision of \vec{L} .

The $B_{\rm tag}$ decay vertex is accurately determined, owing to the collision boost and high-resolution silicon detectors installed at small radial distances from the IR. In the z direction, the $B_{\rm tag}$ -vertex resolution is typically an order of magnitude, or more, smaller than the IR size (see Table I). However, the average $B_{\rm tag}$ flight path—ranging from approximately 130 $\mu{\rm m}$ at Belle II to 260 $\mu{\rm m}$ at BaBar—and its near alignment with the z axis, keeps the decay vertex within the IR ellipsoid. Approximating the resolution on the $B_{\rm tag}$ production point with the IR size would therefore result in a large uncertainty on \vec{L} , spoiling the measurement of $t_{\rm tag}$.

To determine $t_{\rm tag}$, we use instead a topological fit to the coordinates of the measured interaction point $\vec{x}_{\rm IR}$ and $B_{\rm tag}$ decay vertex, $\vec{x}_{\rm tag}$, using their respective covariance

 $^{^{1}}$ If \vec{p}_{CP} cannot be measured, \vec{p}_{tag} can be approximated by the vector sum of the momenta of the B_{tag} decay products. However, since B_{tag} decays are typically reconstructed inclusively to maximize efficiency—and often involve neutrinos—this approximation results in poorer momentum resolution.

matrices, $V_{\rm IR}$ and $V_{\rm tag}$. The covariance matrix $V_{\rm IR}$ is derived from the IR spatial widths, while $V_{\rm tag}$ is determined from the $B_{\rm tag}$ vertex resolution. To mitigate the degradation in precision due to the large IR size, especially along the major axis of the ellipsoid, we incorporate in the fit the known $B_{\rm tag}$ momentum, $\vec{p}_{\rm tag}$, which constrains the flight direction and thereby greatly improves the resolution on \vec{L} . The fit determines the $B_{\rm tag}$ production and decay positions, $\vec{x}_{\rm prod}$ and $\vec{x}_{\rm dec}$, by minimizing the χ^2 function

$$\chi^{2} = (\vec{x}_{\text{prod}} - \vec{x}_{\text{IR}})^{T} V_{\text{IR}}^{-1} (\vec{x}_{\text{prod}} - \vec{x}_{\text{IR}}) + (\vec{x}_{\text{dec}} - \vec{x}_{\text{tag}})^{T} V_{\text{tag}}^{-1} (\vec{x}_{\text{dec}} - \vec{x}_{\text{tag}}),$$
(11)

in which the decay position

$$\vec{x}_{\text{dec}} = \vec{x}_{\text{prod}} + \frac{t_{\text{tag}}}{m_B} \vec{p}_{\text{tag}}$$
 (12)

is a function of t_{tag} through the known B_{tag} momentum. The parameters determined by the fit are \vec{x}_{prod} and t_{tag} (see Appendix A for their analytical derivation). The uncertainty on \vec{p}_{tag} is neglected in Eq. (11) because it is irrelevant. However, it can be introduced by adding a constraint on the momentum in the χ^2 function, for example, when the \vec{p}_{CP} momentum cannot be measured.

Geometrically, the $B_{\rm tag}$ production space-point is identified by the overlap between the IR ellipsoid and a cylinder whose axis is the $B_{\rm tag}$ momentum and whose radius equals the $B_{\rm tag}$ -vertex resolution. The center of this overlap marks the $B_{\rm tag}$ production space-point, and the size of the overlap region defines the resolution (see Fig. 3).

IV. TAG DECAY-TIME RESOLUTION

To investigate the $t_{\rm tag}$ resolution expected at B factory experiments, we generate simplified simulated events according to the decay rates of Eq. (5) and using the parameters of the IR, $B_{\rm tag}$ vertex resolution, and beam energies reported in Table I, to simulate the relevant conditions of each experiment. The energies and momentum magnitudes of the B^0 and \bar{B}^0 mesons in $\Upsilon(4S) \to B^0 \bar{B}^0$ decays are determined from energy-momentum conservation. Their angular distribution follows the known dependence due to the transverse polarization of the $\Upsilon(4S)$ mesons produced in e^+e^- collisions [9]. We do not simulate geometric detector acceptance and neglect resolution effects on the measurement of the B momentum.

We then inspect the distributions of the differences $t_{\rm tag}-t_{\rm tag}^{\rm truth}$ between the $B_{\rm tag}$ decay times $t_{\rm tag}$, reconstructed using Eq. (11), and the true decay times $t_{\rm tag}^{\rm truth}$ (Fig. 4). All distributions are approximately Gaussian with small exponential tails; their core widths provide estimates of the $t_{\rm tag}$ resolutions. The core width is approximately 1.3 ps at Belle II, significantly better than the 6.0 ps figure achieved at previous-generation B factories. To validate our simplified simulation, we also determine

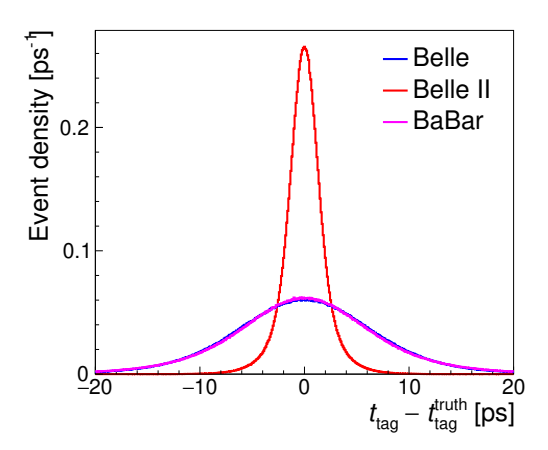


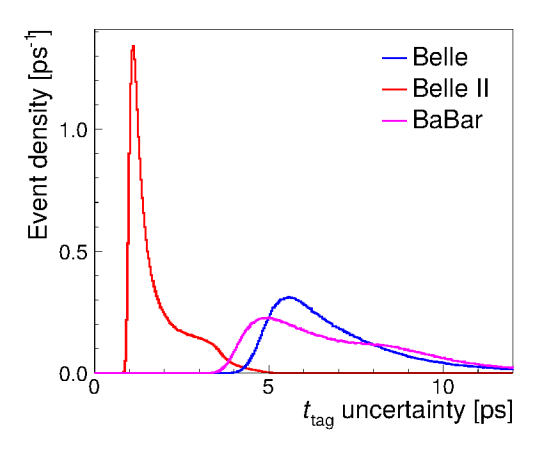
Figure 4. Distribution of simulated $t_{\rm tag}-t_{\rm tag}^{\rm truth}$ obtained from the parameters of Table I for the (blue) Belle-like, (red) Belle II-like, and (magenta) BaBar-like scenarios. The blue and magenta curves overlap.

the Δt resolutions from our model, and find Gaussian-core widths consistent with those observed at Belle II, Belle, and BaBar. Nonetheless, our simplified simulation lacks non-Gaussian tails induced by the charmed-meson lifetimes for $B_{\rm tag}$ vertices from $B \to D$ decays. These tails can lead to an $\mathcal{O}(0.1)$ additional loss in sensitivity to mixing-induced CP violation, which is irrelevant to the conclusions of our study.

The better Belle II performance compared with Belle and BaBar results from four main factors: (i) a smaller IR at SuperKEKB than at KEKB and PEP-II, and (ii) improved $B_{\rm tag}$ vertex resolution. Together, these lead to a smaller intersection between the IR ellipsoid and the $B_{\rm tag}$ tube, enhancing the precision in determining the $B_{\rm tag}$ production space-point. In addition, (iii) a nonzero beam-crossing angle, and (iv) a sufficient boost, jointly increase the fraction of B mesons that exit the IR ellipsoid before decaying at Belle II.²

The minimization of the χ^2 in Eq. (11) also provides a determination of the expected $t_{\rm tag}$ uncertainty $\sigma_{t_{\rm tag}}$, whose distributions are shown in Fig. 5 (left). The resolution varies on an event-by-event basis yielding the distributions of Fig. 4 as integrals over all $t_{\rm tag}$ measurements. When properly estimated, $\sigma_{t_{\rm tag}}$ provides a means to distinguish between events with better or worse time resolution. We validate $\sigma_{t_{\rm tag}}$ as a reliable estimate of the uncertainty on $t_{\rm tag}$ by examining the width of the distribution of $t_{\rm tag}-t_{\rm tag}^{\rm truth}$ as a function of $\sigma_{t_{\rm tag}}$. We observe an accurate correspondence between $\sigma_{t_{\rm tag}}$ and the

² A smaller boost results in B mesons being emitted with a wider angular distribution relative to the boost direction, which reduces the uncertainty of the B_{tag} production point and improves $|\vec{L}|$ resolution. On the other hand, a smaller boost also deteriorates the time resolution by enlarging the denominator of Eq. (A5).



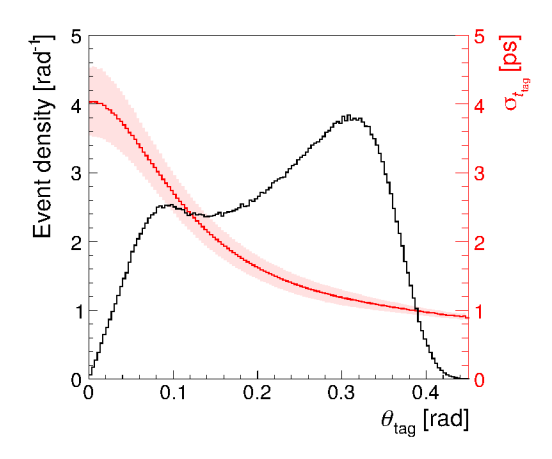


Figure 5. (Left panel) Expected distributions of $\sigma_{t_{\text{tag}}}$ for Belle (blue), Belle II (red), and BaBar (magenta), as obtained from the minimization of the χ^2 function of Eq. (11). (Right panel) distributions of (black) the angle θ_{tag} between the B_{tag} momentum and the z axis and (red) $\sigma_{t_{\text{tag}}}$ as a function of that angle in a Belle II-like scenario. The shaded red band represents the 68.3% confidence interval

width of the $t_{\rm tag}-t_{\rm tag}^{\rm truth}$ distribution, confirming the accuracy of the uncertainty estimate. The resolution $\sigma_{t_{\rm tag}}$ can therefore be used in fits to the time evolution, in analogy with per-event uncertainties in Δt for measurements of $\mathcal{A}_{CP}(\Delta t)$.

The uncertainty $\sigma_{t_{\text{tag}}}$ is independent from $|\hat{L}|$, due to the constraint from the B_{tag} momentum vector in Eq. (12). It depends on the B_{tag} momentum-vector direction though (see Fig. 5 (right)). The more \vec{p}_{tag} is collinear with the main axis of the IR ellipsoid, the larger the intersection between the IR and the B_{tag} tube, hence the uncertainty on the production space-point and t_{tag} ; the closer \vec{p}_{tag} is to the transverse plane, the smaller the intersection and thus the uncertainty. The dependence on the direction generates the bimodal shape of the $\sigma_{t_{tag}}$ distribution in a Belle II-like scenario. In the same scenario, minimizing the χ^2 of Eq. (11) with the \vec{p}_{tag} constraint improves the t_{tag} resolution by a factor of about three, compared to using the IR center as the B_{tag} production space-point, i.e., when t_{tag} is reconstructed directly by Eq. (10) without performing the vertex fit.

From the distribution of $\sigma_{t_{\text{tag}}}$, we compute an effective time resolution, $\sigma_{t_{\text{tag}}}^{\text{eff}}$, which corresponds to the width of the single-Gaussian resolution that yields the same sensitivity on the CP-violating coefficient S as that obtained considering all values of $\sigma_{t_{\text{tag}}}$. We combine the uncertainties $\sigma_{S}(\sigma_{t_{\text{tag}}})$ on S, from the function in Fig. 2, weighted with the normalized distribution $w(\sigma_{t_{\text{tag}}})$ of $\sigma_{t_{\text{tag}}}$, *i.e.*,

$$\frac{1}{\sigma_S^2(\sigma_{t_{\text{tag}}}^{\text{eff}})} = \int \frac{w(\sigma_{t_{\text{tag}}})}{\sigma_S^2(\sigma_{t_{\text{tag}}})} d\sigma_{t_{\text{tag}}}.$$
 (13)

The resulting effective $t_{\rm tag}$ resolutions are 1.5 ps at Belle II, 6.3 ps at Belle, and 6.0 ps at BaBar. With respect to the case with perfect $t_{\rm tag}$ resolution, the precision of S is therefore expected to reduce by a factor of 1.7 for Belle II, 8.0 for Belle, and 7.0 for BaBar, due to the time-resolution-dependent dilution of the asymmetry

(see, e.g., Fig. 2). These findings show that measurements of time-dependent *CP* asymmetry without signal vertex only are feasible and competitive at Belle II.

V. CASE STUDY: $B^0 \to \pi^0 \pi^0$ AND IMPACT ON THE CKM ANGLE ϕ_2

To assess the potential impact quantitatively, we apply our method to a realistic use case, a measurement of time-dependent CP-violating asymmetries in $B^0 \to \pi^0\pi^0$ decays at Belle II. If available, this measurement could significantly improve the determination of the CKM angle $\phi_2 = \arg(V_{td}V_{tb}^*/V_{ud}V_{ub}^*)$, where V_{ij} are CKM matrix elements, enhancing in turn the constraining power of CKM-unitarity tests. Prior to using our approach to determine mixing-induced CP violation in $B^0 \to \pi^0\pi^0$ decays, which is unknown, a consistency check based on $B^0 \to J/\psi K^0$ decays would provide a high-precision validation.

The angle ϕ_2 is typically constrained through a combination of results from decays related by isospin symmetry, $B^0 \to \pi^+\pi^-$, $B^+ \to \pi^+\pi^0$, and $B^0 \to \pi^0\pi^0$. This combination suppresses hadronic uncertainties due to penguin contributions in the $B^0 \to \pi^+\pi^-$ decay amplitude [24]. The current 4.5° precision on ϕ_2 is driven by the precision of an independent determination based on an analogous isospin analysis of $B \to \rho \rho$ decays. The $B \to \pi\pi$ analysis is less impactful also because it yields degenerate results due to an eight-fold ambiguity. The degeneracy originates from lack of experimental information on mixing-induced CP violation in $B^0 \to \pi^0 \pi^0$ decays, typically denoted with the S_{00} coefficient. To date, a measurement of S_{00} has been considered feasible by only reconstructing the $\pi^0 \to e^+e^-\gamma$ final state to enable signal-vertex reconstruction and the ensuing Δt measurement. However, this standard approach requires

datasets 50–100 times larger than those currently available [25, 26]. We show that a measurement of $\mathcal{A}'_{CP}(t_{\text{tag}})$ yields highly constraining S_{00} information by already using the data collected by Belle II thus far.

We build upon the recent measurement of the $B^0 \to \pi^0\pi^0$ branching fraction and time-integrated CP-violating asymmetry C_{00} , in which 126 signal decays were reconstructed in the Belle II sample collected until 2022, and corresponding to an integrated luminosity of 362 fb⁻¹ [27]. We assume the same sample size and composition as in Ref. [27]. The sample is background-dominated: approximately 6850 events are from light-quark production processes (continuum) and 170 from other B decays ($B\overline{B}$ background), such as $B^+ \to \rho^+(\to \pi^+\pi^0)\pi^0$, where the π^+ is not reconstructed.

The results in Ref. [27] were obtained from a fit to three background-discriminating observables (ΔE , $M_{\rm bc}$, and C_t) and one flavor-sensitive observable (w_t). The first observable is the difference between the B-candidate energy and half of the beam energy, $\Delta E = E_B^* - E_{\rm beam}^*$; the second observable is the B-candidate mass calculated from the B momentum and the beam energy, $M_{\rm bc} = \sqrt{E_{\rm beam}^{*2} - p_B^{*2}}$; the third observable, C_t , is the transformed output of a classifier trained to suppress continuum; and the fourth observable, w_t , is the transformed fraction of incorrectly tagged events w_t , estimated by a flavor-tagging algorithm providing the $B_{\rm tag}$ flavor q [14]. All starred quantities are calculated in the center-of-mass frame.

We generate simplified simulated data by sampling the probability density function (PDF) used in Ref. [27], extended to include the observables $t_{\rm tag}$ and $\sigma_{t_{\rm tag}}$. Unlike in Ref. [27], we assume that the joint PDF factorizes as the product of the individual PDFs for each observable; in addition, we neglect flavor-tagging asymmetries and uncertainties on the flavor-tagging parameters. These approximations are not expected to bias appreciably the expected resolutions on the fit results, thus not compromising the validity of this study. The full PDF is

$$\mathcal{P}(t_{\text{tag}}, \sigma_{t_{\text{tag}}}, \Delta E, M_{\text{bc}}, C_t, w_t, q) = \sum_{j} f_j \mathcal{P}_j(t_{\text{tag}}, \sigma_{t_{\text{tag}}}; q, w) \mathcal{P}_j(\Delta E) \mathcal{P}_j(M_{\text{bc}}) \mathcal{P}_j(C_t) \mathcal{P}_j(w_t),$$
(14)

where f_j is the fraction of component j, an index that indicate signal (s), continuum (c) or $B\overline{B}$ background (b), and f_b equals $1 - f_s - f_c$.

The PDFs for ΔE , $M_{\rm bc}$, C_t , and w_t are taken from Ref. [27]. Integrating Eq. (14) over $t_{\rm tag}$ and $\sigma_{t_{\rm tag}}$ yields the time-integrated model used in that reference. To validate our implementation, we fit to the simulated data generated from this model to determine signal fraction, continuum fraction, and C_{00} . The fit yields unbiased results with Gaussian uncertainties. The average statistical uncertainty of C_{00} equals 0.28 \pm 0.02, consistent with the 0.30 value reported in Ref. [27].

In the time-dependent analysis, the signal PDF derives from Eq. (5) after incorporating the effect of the wrongtag fraction w, and the convolution with a Gaussian time-resolution model $\mathcal{R}_{\sigma_{t_{\text{tag}}}}$,

$$\mathcal{P}_{s}(t_{\text{tag}}, \sigma_{t_{\text{tag}}}; q, w) = \frac{e^{-t'_{\text{tag}}/\tau}}{2\tau} \left(1 + q(1 - 2w) \left[S' \sin \Delta m(t'_{\text{tag}} - \hat{t}) \right] - C' \cos \Delta m(t'_{\text{tag}} - \hat{t}) \right] \right) \otimes \mathcal{R}_{\sigma_{t_{\text{tag}}}}(t_{\text{tag}} - t'_{\text{tag}}).$$
(15)

Here, $\sigma_{t_{\text{tag}}}$ indicates the per-event tag decay-time resolution, which effectively increases the importance of events with better resolution in the fit. The physical CP-violating parameters S_{00} and C_{00} are related to S' and C' via Eq. (8).

For backgrounds, we use a δ -function distribution for continuum, and an exponential decay with the B^+ lifetime for the $B\overline{B}$ component. This is motivated by the dominance of the $B^+ \to \rho^+ \pi^0$ contribution reported in Ref. [27]. Both are convolved with the same Gaussian resolution as the signal. We assume the $\sigma_{t_{\rm tag}}$ distribution is the same across components.

We simulate three scenarios, (i) the 365 fb⁻¹ dataset that Belle II collected up to 2022, (ii) an intermediate sample corresponding to 5 ab⁻¹, and (iii) the design full dataset of 50 ab⁻¹. These assess the feasibility, mid-term reach, and ultimate sensitivity, respectively, of our approach in a Belle II-like experiment. In each case, simulated data are generated assuming $S_{00} = 0.65$, which is the value favored by an indirect ϕ_2 determination [28], and $C_{00} = 0.00$, which is compatible with current determinations from time-integrated measurements and allows assessing more directly the impact on mixing-induced CP violation. For each scenario, we fit simulated data to determine the signal and continuum fractions, S_{00} , and C_{00} .

An example of the background-subtracted $t_{\rm tag}$ distribution for B^0 - and \overline{B}^0 -tagged decays and the corresponding asymmetry, with fit projections overlaid, is shown in Fig. 6. All estimates are unbiased and have Gaussian uncertainties. The resulting average statistical uncertainties for S_{00} and C_{00} are listed in Table II. Simulation shows that the sensitivities to S_{00} and C_{00} do not depend on the assumed values of these parameters. In that table, we also compare our results with those from the standard method using Δt from $e^+e^-\gamma$ vertexing, following Ref. [26]. The projected uncertainty on S_{00} from our method for the ultimate sample size scenario

Sample size	$t_{ m tag}$	Δt
$[{ m ab}^{-1}]$	$\sigma_{S_{00}}$ $\sigma_{C_{00}}$	$\sigma_{S_{00}}$
0.36	$0.75 \ 0.27$	_
5	$0.18 \ 0.07$	_
50	$0.06 \ 0.02$	0.28

Table II. Expected statistical uncertainties on S_{00} and C_{00} from $t_{\rm tag}$ -dependent analyses in the various Belle II-like scenarios, compared with the S_{00} uncertainty expected in the standard Δt analysis [26].

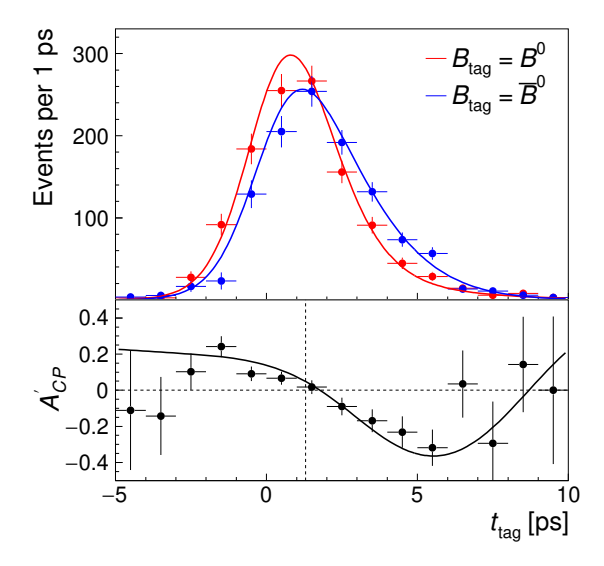


Figure 6. (Top panel) example of a background-subtracted $t_{\rm tag}$ distributions for (red) B^0 and (blue) \overline{B}^0 mesons and (bottom panel) corresponding decay-rate asymmetry in a Belle II-like 50 ab⁻¹ scenario, with fit projections overlaid. Simulated data are displayed in the signal-enhanced region $-0.10 < \Delta E < 0.05\,{\rm GeV},\,5.275 < M_{\rm bc} < 5.285\,{\rm GeV},\,C_t > 0$. In addition, we apply w < 0.2 and $\sigma_{t_{\rm tag}} < 2\,{\rm ps}$ for enhancing visualization of the asymmetry. Corresponding fit results are $S_{00} = 0.69 \pm 0.06$ and $C_{00} = 0.00 \pm 0.02$.

is 0.06, approximately five times smaller than the 0.28 reported in Ref. [26] for the standard method. Our approach achieves the same sensitivity with approximately 2 ab⁻¹, which would be a 20-times smaller dataset.

These findings show promising potential for the determination of ϕ_2 . We assess the potential impact from a $B \to \pi\pi$ isospin analysis that incorporates our projected results in addition to the existing inputs for three cases: (i) using all $B \to \pi\pi$ measurements available to date; (ii) combining all $B \to \pi\pi$ measurements available to date with the S_{00} results expected from our method in a Belle II-like scenario based on the 0.36 ab⁻¹ sample collected up to 2022; and (iii) combining all $B \to \pi\pi$ measurements available to date with the projected S_{00} determination for a Belle II-like scenario with 5 ab⁻¹ We use values of branching fractions for $B^0 \to \pi^+\pi^-$, $B^+ \to \pi^+ \pi^0$, and $B^0 \to \pi^0 \pi^0$ decays, B-meson lifetimes, and the *CP*-violating coefficients S_{+-} , C_{+-} , S_{00} , and C_{00} as inputs, following the analysis of Ref. [24]. We use $S_{00} = 0.65 \pm 0.75 \ (0.65 \pm 0.18)$ in the $0.36 \ (5) \,\mathrm{ab^{-1}}$ sample for the unknown value of the mixing-induced CPviolation coefficient, in which the central value follows Ref. [28] and the uncertainties are from Table II. We use known values for all other inputs [5]. The Belle II results in Ref. [27] are assumed uncorrelated with S_{00} . While the details of the ϕ_2 results depend moderately on these choices, the general conclusions are expected to hold. To assess the sole impact of our method, all inputs except

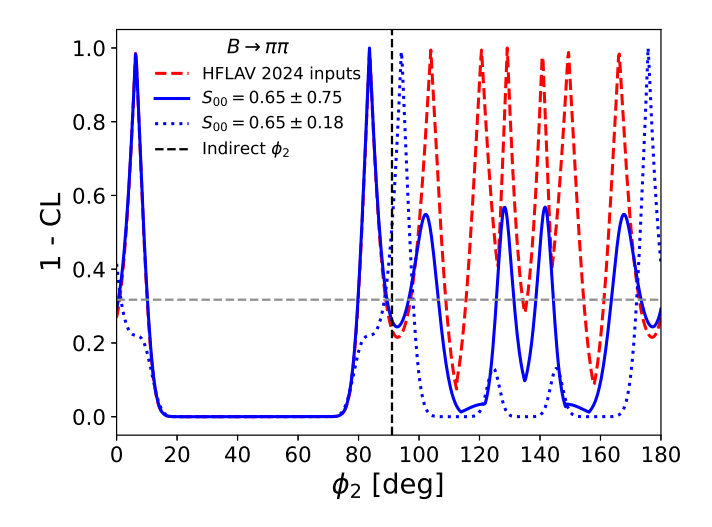


Figure 7. P-value as a function of the CKM angle ϕ_2 from an isospin-based combination of (red dashed) all currently available $B \to \pi\pi$ results only, (blue solid) all currently available results and $B^0 \to \pi^0\pi^0$ results expected from this approach in a Belle II-like scenario based on the 0.36 ab⁻¹ sample collected up to 2022, and (blue dashed) all current results and Belle II-like $B^0 \to \pi^0\pi^0$ results expected from this approach in an hypothetical $5\,\text{ab}^{-1}$ sample. All other inputs are the latest known values [5].

for S_{00} are kept unchanged in all scenarios, although the precision on most of them is expected to improve as well.

Figure 7 shows the results of the isospin analysis. Resulting p-values as functions of ϕ_2 are displayed. Already with the Belle II sample collected up to 2022, the results enabled by our method would reduce the solution degeneracy from eight solutions to two, and would reduce the 68% confidence-level interval around the solution favored by global fits. This demonstrates that a $t_{\rm tag}$ -based time-dependent analysis of $B^0 \to \pi^0 \pi^0$ significantly improves the global determination of ϕ_2 .

VI. SUMMARY

We develop a method that enables measurement of time-dependent CP-violation in B^0 mesons produced in energy-asymmetric electron-positron collisions near the $\Upsilon(4S)$ resonance and reconstructed without a signal vertex. The relevant time-evolution is expressed solely as a function of the decay time of the pair-produced tag-B meson and information on signal CP violation is provided by the quantum correlation of the $B^0\overline{B}^0$ pair. Key is a compact e^+e^- interaction region and excellent vertex resolution, which enable precise measurement of the tag-B decay time. This approach extends and enhances sensitivity to time-dependent CP-violating parameters in decays without charged particles, such as those involving only π^0 , K^0 , and photons in the final state. When applied to the $B^0 \to \pi^0 \pi^0$ decay, for instance, simulation

shows that the method achieves a sensitivity on mixing-induced CP violation that would require 20-times larger samples with standard approaches. This implies that meaningful constraints on the CP-violating coefficients S and C can already be achieved for $B^0 \to \pi^0 \pi^0$ decays with the current $0.5~{\rm ab}^{-1}$ Belle II sample. The expected sensitivity on S would reduce the degeneracy of solutions for the CKM angle ϕ_2 in the isospin analysis of $B \to \pi\pi$ decays, substantially improving its determination. These findings establish the $t_{\rm tag}$ -dependent analysis as a powerful enabler for precision CP-violation studies at Belle II and beyond.

Appendix A: Formulas for tag-side vertexing

The linearity of the χ^2 regression of Eq. (11) allows to derive explicit analytic expressions for the best-fit vertex positions, $t_{\rm tag}$ times, and $\sigma_{t_{\rm tag}}$ uncertainties. We introduce the vector $\vec{n} = \vec{p}_{\rm tag}/m_B$ to simplify the algebra along with

$$E = (V_{\rm IR}^{-1} + V_{\rm tag}^{-1})^{-1},$$

$$\vec{x}_m = E(V_{\rm IR}^{-1} \vec{x}_{\rm IR} + V_{\rm tag}^{-1} \vec{x}_{\rm tag}).$$
(A1)

We obtain the tag decay time

$$t_{\text{tag}} = \frac{\vec{n}^T V_{\text{tag}}^{-1}(\vec{x}_m - \vec{x}_{\text{tag}})}{\vec{n}^T (V_{\text{tag}}^{-1} E V_{\text{tag}}^{-1} - V_{\text{tag}}^{-1}) \vec{n}},$$
(A2)

- M. Kobayashi and T. Maskawa, Prog. Theor. Phys. 49, 652 (1973).
- [2] B. Aubert et al. (BaBar Collaboration), Phys. Rev. Lett. 87, 091801 (2001).
- [3] K. Abe et al. (Belle Collaboration), Phys. Rev. Lett. 87, 091802 (2001).
- [4] R. Fleischer, Eur. Phys. J. Special Topics 233, 391 (2024).
- [5] S. Banerjee et al. (Heavy Flavor Averaging Group), (2024), arXiv:2411.18639 [hep-ex], and online updates at https://hflav.web.cern.ch.
- [6] T. Affolder et al. (CDF Collaboration), Phys. Rev. D 61, 072005 (2000).
- [7] R. Aaij et al. (LHCb Collaboration), Eur. Phys. J. C 72, 2022 (2012).
- [8] R. Aaij et al. (LHCb Collaboration), Eur. Phys. J. C 77, 238 (2017).
- [9] A. J. Bevan *et al.* (BaBar and Belle Collaborations), Eur. Phys. J. C74, 3026 (2014).
- [10] A. D. Foland, Phys. Rev. D 60, 111301 (1999).
- [11] D. Boutigny et al. (BaBar Collaboration), SLAC-R-0504 (1998).
- [12] S. Navas et al. (Particle Data Group), Phys. Rev. D 110, 030001 (2024).

and the production and decay vertices determined from the fit are then expressed as

$$\vec{x}_{\text{prod}} = \vec{x}_m - t_{\text{tag}} E V_{\text{tag}}^{-1} \vec{n},$$

$$\vec{x}_{\text{dec}} = \vec{x}_{\text{prod}} + t_{\text{tag}} \vec{n}.$$
(A3)

The tag decay time calculated using $t_{\text{tag}} = m_B \vec{p}_{\text{tag}} \cdot (\vec{x}_{\text{dec}} - \vec{x}_{\text{prod}})/|\vec{p}_{\text{tag}}|^2$ is identical to the value resulting from Eq. (A2).

The inverse variance of $t_{\rm tag}$ as determined from the fit is

$$\frac{1}{\sigma_{t_{\text{tag}}}^{2}} = (EV_{\text{tag}}^{-1}\vec{n})^{T}V_{\text{IR}}^{-1}(EV_{\text{tag}}^{-1}\vec{n})
+ (EV_{\text{tag}}^{-1}\vec{n} - \vec{n})^{T}V_{\text{tag}}^{-1}(EV_{\text{tag}}^{-1}\vec{n} - \vec{n})$$
(A4)

In the limit of isotropic B_{tag} vertex resolution σ_{tag} and an elongated interaction region, the t_{tag} resolution approximates to

$$\sigma_{t_{\rm tag}} \approx \frac{\sqrt{\sigma_{{\rm IR}_{xy}}^2 + \sigma_{\rm tag}^2}}{(\beta \gamma)_{\rm tag} \sin \theta_{\rm tag}},$$
 (A5)

where $\sigma_{\text{IR}_{xy}}$ is the transverse size of the interaction region, $(\beta\gamma)_{\text{tag}}$ is the boost of the B_{tag} meson, and θ_{tag} is the angle between \vec{p}_{tag} and the main axis of the interaction region.

ACKNOWLEDGMENTS

We thank A. Di Canto, T. Gershon, and J. Libby for useful suggestions on the manuscript.

- [13] O. Long, M. Baak, R. N. Cahn, and D. P. Kirkby, Phys. Rev. D 68, 034010 (2003).
- [14] I. Adachi et al. (Belle II Collaboration), Phys. Rev. D 110, 012001 (2024).
- [15] H. G. Moser and A. Roussarie, Nucl. Instrum. Meth. A 384, 491 (1997).
- [16] H. Tajima et al., Nucl. Instrum. Meth. A 533, 370 (2004).
- [17] B. Aubert et al. (BaBar Collaboration), Phys. Rev. D 66, 032003 (2002).
- [18] W. Kozanecki, A. J. Bevan, B. F. Viaud, Y. Cai, A. S. Fisher, C. O'Grady, B. Lindquist, A. Roodman, J. M. Thompson, and M. Weaver, Nucl. Instrum. Meth. A 607, 293 (2009).
- [19] Y. Ohnishi et al., Prog. Theor. Exp. Phys. 2013, 03A011 (2013).
- [20] N. Toge, KEK-Report-95-7 (1995).
- [21] R. Žlebčík, in Proceedings of Connecting The Dots (CTD2022) (2023).
- [22] R. Mizuk *et al.* (Belle Collaboration), J. High Energy Phys. **06**, 137 (2021).
- [23] B. Aubert *et al.* (BaBar Collaboration), Phys. Rev. D 72, 032005 (2005).
- [24] M. Gronau and D. London, Phys. Rev. Lett. 65, 3381 (1990).

- [25] H. Ishino, M. Hazumi, M. Nakao, $\,$ and T. Yoshikawa, $\,$ (2007), arXiv:hep-ex/0703039.
- [26] W. Altmannshofer et al., Prog. Theor. Exp. Phys. 2019, 123C01 (2019), [Erratum: Prog. Theor. Exp. Phys. 2020,
- 029201 (2020)].
- [27] I. Adachi et al. (Belle II Collaboration), Phys. Rev. D 111, L071102 (2025).
- [28] J. Charles, O. Deschamps, S. Descotes-Genon, and V. Niess, Eur. Phys. J. C 77, 574 (2017).